

Discovery of an old nova shell surrounding the cataclysmic variable V1315 Aql

D. I. Sahman,^{1*} V. S. Dhillon,^{1,2*} S. P. Littlefair,¹ and G. Hallinan³

¹*Department of Physics and Astronomy, University of Sheffield, Sheffield S3 7RH, UK*

²*Instituto de Astrofísica de Canarias, E-38205 La Laguna, Tenerife, Spain*

³*California Institute of Technology, 1200 East California Boulevard, Pasadena, California 91125, USA*

Accepted 2018 April 12. Received 2018 March 19

ABSTRACT

Following our tentative discovery of a faint shell around V1315 Aql reported in Sahman et al. (2015), we undertook deep H α imaging and intermediate-resolution spectroscopy of the shell. We find that the shell has its geometric centre located on V1315 Aql. The mass, spectral features and density of the shell are consistent with other nova shells, rather than planetary nebulae or supernova remnants. The radial velocity of the shell is consistent with the systemic velocity of V1315 Aql. We believe this evidence strongly suggests that the shell originates from an earlier nova event. This is the first nova shell discovered around a novalike, and supports the theory of nova-induced cycles in mass transfer rates (hibernation theory) first proposed by Shara et al. (1986).

Key words: stars: – novae – cataclysmic variables.

1 INTRODUCTION

Cataclysmic variables (CVs) are close binary systems in which a white dwarf (WD) primary accretes material from a late-type secondary star, via Roche-lobe overflow (see Warner 1995 for a review). Non-magnetic CVs are classified into 3 main sub-types – the novae, the dwarf novae and the nova-likes. The *novae* are defined as systems in which only a single nova eruption has been observed. Novae eruptions have typical amplitudes of 10 magnitudes and are believed to be due to the thermonuclear runaway of hydrogen-rich material accreted onto the surface of the white dwarf. The *dwarf novae* (DNe) are defined as systems which undergo quasi-regular (on timescales of weeks–months) outbursts of much smaller amplitude (typically 6 magnitudes). Dwarf novae outbursts are believed to be due to instabilities in the accretion disc causing it to collapse onto the white dwarf. The *nova-like* variables (NLs) are the non-eruptive CVs, i.e. objects which have never been observed to show novae or dwarf novae outbursts. The absence of dwarf novae outbursts in NLs is believed to be due to their high mass-transfer rates, producing ionised accretion discs in which the disc-instability mechanism that causes outbursts is suppressed (Osaki 1974); the mass transfer rates in NLs are

$\dot{M} \sim 10^{-9} M_{\odot} \text{ yr}^{-1}$ whereas DNe have rates of $\dot{M} \sim 10^{-11} M_{\odot} \text{ yr}^{-1}$ (Warner 1995).

Our understanding of CV evolution has made great strides in recent years (e.g. Knigge 2010, Knigge et al. 2011). However, one of the main unsolved problems in CV evolution is: how can the different types of CV co-exist at the same orbital period? Theory predicts that all CVs evolve from longer to shorter orbital periods on timescales of gigayears, and as they do so the mass-transfer rate also declines. At periods longer than approximately 5 hours, all CVs should have high mass-transfer rates and appear as nova-likes, whereas below this period the lower mass-transfer rate allows the disc-instability mechanism to operate and all CVs should appear as dwarf novae (Knigge et al. 2011). This theoretical expectation, however, is in stark contrast to observations, which show that nova-likes are far more common than dwarf novae in the 3–4 hr period range (Rodríguez-Gil et al. 2007).

Two possible explanations for the coexistence of nova-likes and dwarf novae at the same orbital periods have been proposed, both of which invoke cycles in \dot{M} on timescales shorter than the gigayear evolutionary timescale of CVs. The first explanation is that the \dot{M} cycles are caused by irradiation from the accreting WD, which bloats the secondary and hence increases \dot{M} (e.g. Büning & Ritter 2004). Knigge et al. (2011) found that irradiation would cause bloating of <3% above the period gap, leading to modest fluctuations

* E-mail: d.sahman@sheffield.ac.uk; vik.dhillon@sheffield.ac.uk

in \dot{M} with timescales of the order of $10^6 - 10^9$ yr, insufficient to explain the full range in \dot{M} that is observed. The second explanation for variable \dot{M} is a nova-induced cycle. Some fraction of the energy released in the nova event will heat up the WD, leading to irradiation and subsequent bloating of the secondary. Following the nova event, the system would have a high \dot{M} and appear as a NL. As the WD cools, \dot{M} reduces and the system changes to a DN, or even possibly \dot{M} ceases altogether and the system goes into hibernation. Hence CVs are expected to cycle between nova, NL and DN states, on timescales of $10^4 - 10^5$ yrs (see Shara et al. 1986).

The cyclical evolution of CVs through nova, NL and DN phases recently received observational support from the discovery that BK Lyn appears to have evolved through all three phases since its likely nova outburst in the year AD 101 (Patterson et al. 2013). A second piece of evidence has come from the discovery of nova shells around the dwarf novae Z Cam and AT Cnc (Shara et al. 2007, Shara et al. 2012), verifying that they must have passed through an earlier nova phase. Shara et al. (2017) also found a nova shell from Nova Sco 1437 and were able to associate it with a nearby dwarf nova using its proper motion. A more obvious place than DNe to find nova shells is actually around NLs, as the nova-induced cycle theory suggests that the high \dot{M} in NLs is due to a recent nova outburst. Finding shells around NLs would lend further support to the existence of nova-induced cycles and hence why systems with different \dot{M} are found at the same orbital period.

In our earlier paper (Sahman et al. 2015; hereafter S15), we presented the initial results of our search for nova shells around CVs. We reported the tentative discovery of a possible shell around the nova-like V1315 Aql (orbital period 3.35 hr). We subsequently obtained intermediate-resolution spectroscopy of this shell, in an effort to determine its physical characteristics and to ascertain if it is associated with the nova-like. The results of these spectroscopic observations, along with a more in-depth analysis of the H α images of the V1315 Aql shell shown in S15, are presented in this paper.

2 OBSERVATIONS AND DATA REDUCTION

2.1 Observations

2.1.1 INT images

We used the Wide Field Camera¹ at the prime focus of the 2.5m Isaac Newton Telescope on La Palma to image V1315 Aql on the night of 2014 August 2. This setup gave a platescale of 0.33"/pixel and a field view of approx. 34' \times 34'. H α is generally the strongest feature in the spectra of nova shells, with a velocity width of up to 2000 km s⁻¹ (e.g. Duerbeck & Seitter 1987). In order to maximise the detection of light from the shell and minimise the contribution of sky, we therefore used a narrow-band (95Å FWHM = 4300 km s⁻¹) interference filter centred on the rest wavelength of H α (ING filter number 197²). We took eight 900s H α exposures, with four of the images dithered by $\pm 20''$ in both RA and Dec. The observing conditions were good throughout the run: the

sky was always photometric, there was no evidence of dust and the seeing was 1.5".

2.1.2 Keck DEIMOS spectra

We used the DEIMOS (Faber et al. 2003) multi-slit spectrograph on the 10m Keck II telescope on Hawaii, on the night of 2015 June 13. We obtained 39 spectra of 300s duration each, using the 1200G grating centred on 6000Å and the GG455 order-blocking filter. This gave a wavelength coverage of 4550–7500Å, with a FWHM resolution of 1.6Å. The seeing was 0.7", and there was some thin cloud present.

The slit mask design requires that the slits cannot overlap in the spatial direction, so we placed seven slits around the edges of the roughly circular shell. We also placed a slit on V1315 Aql itself and chose four nearby stars for flux calibration. We identified two areas of blank sky for sky subtraction. The positions of each slit on the sky are shown in Figure 2, and full details of the position, orientation and wavelength coverage of each slit are given in Table 1.

2.1.3 0.5m Telescope – La Palma

Our Keck spectra included four stars for flux calibration but unfortunately they did not appear in any photometric catalogues. In order to allow us to perform flux calibration, we therefore obtained additional images of the four stars together with two catalogue stars (TYC 1049-408-1 and IPHAS J1911411.93+121357.7) using the 0.5m robotic telescope *pt5m* on La Palma (Hardy et al. 2015). The observations were taken on 2016 October 7, when we took four images in each of the *B*, *V*, *R*, *I* filters with an exposure time of 1 minute each, and on 2016 Nov 18, when we took four 40 sec *R*-band images and four 360 sec *B*-band images.

2.2 Data reduction

2.2.1 INT images

The INT images were debiased using the median level of the overscan strip and flat-fielded using normalised twilight sky flats. All image processing was carried out using THELI³. Figure 1 shows the final stacked image of the shell.

2.2.2 Keck DEIMOS spectra

We used IRAF to reduce the DEIMOS spectra. The spectra were bias corrected using the overscan strip on the chips, and were flat-fielded using quartz lamp flats. We had difficulty in performing the background sky subtraction because the two blank sky slits we had chosen both contain small residual H α emission lines, possibly from the nova shell.

We then tried using the sky portion of our four flux calibration stars, but we found that the spectra of the three closest to the shell (Stars 1–3) also contained low levels of residual H α emission. (See Figure 5). The best results were obtained with sky from Star 4, which is furthest from the

¹ <http://www.ing.iac.es/astrometry/instruments/wfc/>

² <http://catserver.ing.iac.es/filter/list.php?instrument=WFC>

³ <http://www.ing.iac.es/astrometry/instruments/wfc/WFC-THELI-reduction.html>

Table 1. V1315 Aql DEIMOS slit positions, sizes and spectral range coverage. The RA and Dec positions are for the centres of the slits.

Slit name	RA (degs)	Dec (degs)	Slit Length (arcsecs)	Slit Position angle (degs)	Slit Width (arcsecs)	Wavelength range	
						Start(Å)	End (Å)
Blank Sky 1	288.5230602	12.2217710	58.872	154.4	0.7	4780	7432
Blank Sky 2	288.4896981	12.3217610	49.423	154.4	0.7	4867	7514
Shell 1	288.4995975	12.3003892	32.904	154.4	1.0	4868	7521
Shell 2	288.5116182	12.2922447	46.933	150.0	1.0	4915	7576
Shell 3	288.4560525	12.3369014	74.181	170.0	1.0	4686	7342
Shell 4	288.4507472	12.3566674	65.419	170.0	1.0	4699	7343
Shell 5	288.5171327	12.2647206	59.595	154.4	1.0	4877	7529
Shell 6	288.4757487	12.2611586	43.389	150.0	1.0	4614	7272
Shell 7	288.4367229	12.3103574	43.386	130.0	1.0	4487	7170
V1315 Aql	288.4769928	12.3013719	42.173	154.4	1.0	4735	7382
Star 1	288.5492156	12.2172214	49.155	154.4	1.0	5058	7565
Star 2	288.5403078	12.2461305	45.629	154.4	1.0	5047	7592
Star 3	288.5135945	12.2472213	42.009	154.4	1.0	4898	7455
Star 4	288.5604882	12.2053443	61.154	154.4	1.0	5038	7586

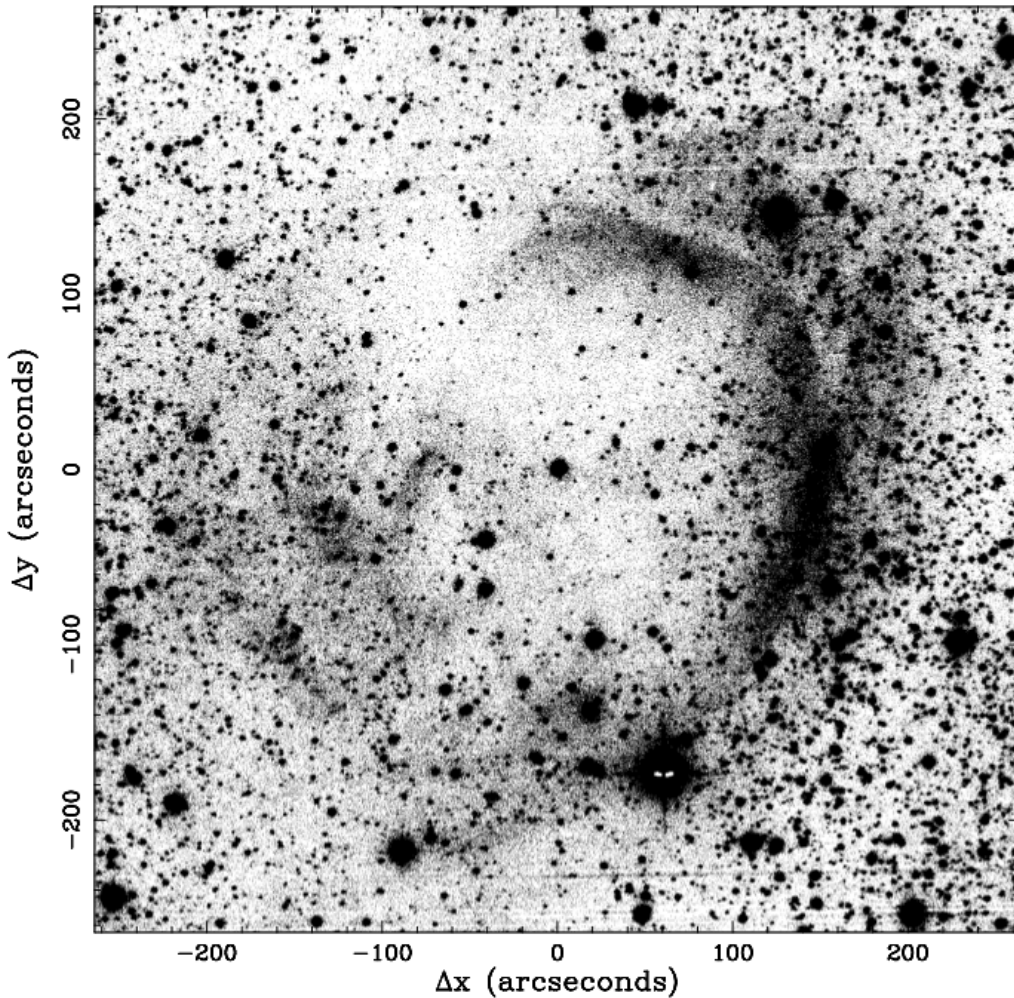


Figure 1. INT WFC H α image of the nova shell around V1315 Aql. The binary is located at the centre of the image. North is up and East is left.

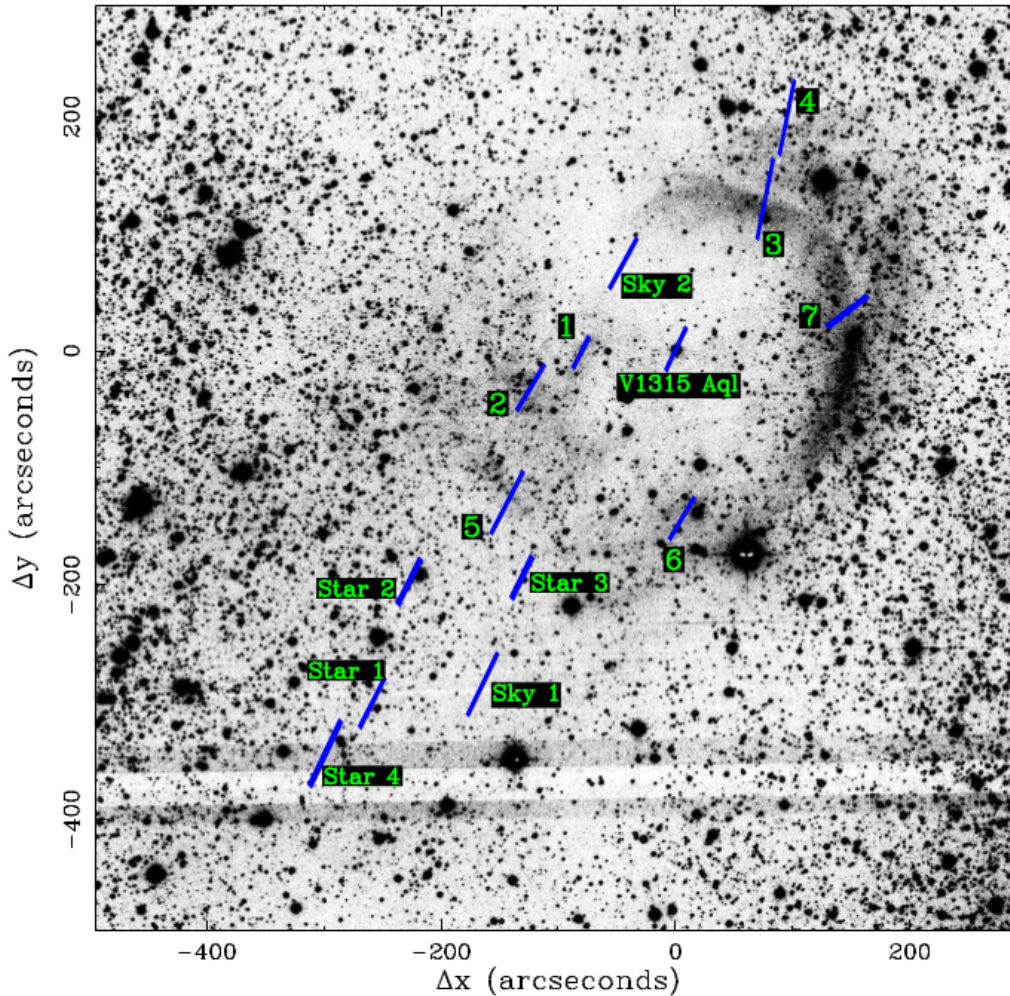


Figure 2. INT WFC $H\alpha$ image of the nova shell around V1315 Aql with the Keck DEIMOS slit positions and sizes overlaid. V1315 Aql is situated at $x=0$, $y=0$. The seven shell slits are numbered, and the two blank sky slits are also shown. The four flux calibration stars are marked Star 1–4. North is up and East is left. The horizontal band across the image at $y \sim -380$ is the gap between two of the CCDs in the WFC mosaic.

shell and showed negligible $H\alpha$ emission – this was used for all subsequent background sky subtraction.

2.2.3 *pt5m images*

The images were bias and flat field corrected using standard IRAF procedures. This allowed us to derive magnitudes for the four flux calibration stars, as shown in Table 2. We also found 2MASS infrared magnitudes (Skrutskie et al. 2006) for Star 2. Hence, the star with the most complete set of magnitudes was Star 2. We input these values into the Virtual Observatory SED Analyser (VOSA – see Bayo et al. 2008) to determine the spectral type of Star 2, obtaining M4V (± 2). We then used VOSA to generate a template spectrum of an M4V star, which we used to flux calibrate the Keck spectra in IRAF.

2.2.4 *Review of satellite imagery*

We searched the GALEX UV satellite footprint using the GalexView interface (Bianchi 2014), but no observations

Table 2. Magnitudes of the four flux-calibration stars observed with Keck DEIMOS. The errors on the B , V , R , I magnitudes are ± 0.3 magnitudes. See Table 1 for the positions of the stars on the sky.

Band	Star 1	Star 2	Star 3	Star 4
B	18.8	16.5	–	–
V	17.6	15.3	19.5	18.3
R	16.9	14.5	18.4	16.5
I	15.1	13.7	17.2	14.6
2MASS J	–	12.508	–	–
2MASS H	–	11.798	–	–
2MASS K	–	11.646	–	–

were taken of the field around V1315 Aql. We also examined the WISE $22\mu\text{m}$ data (Wright et al. 2010), and there was no emission in the vicinity of V1315 Aql.

3 RESULTS

3.1 INT image

The H α image of the shell surrounding V1315 Aql is shown in Figure 1. The images clearly show one, possibly two roughly spherical shells centred on V1315 Aql. The lobe towards the West has the most prominent emission. There was no evidence of nebulosity on wider scales than shown in Figure 2.

There is a possibility that the shell is unrelated to V1315 Aql, and it may just be a line-of-sight alignment of a foreground or background cloud of gas in the Milky Way. To determine that the shell does indeed originate from V1315 Aql, we need to determine if it has the same systemic velocity as the binary, and that its composition is comparable to other nova shells, and to rule out other types of nebulosity, e.g. planetary nebulae, supernovae remnants.

3.2 Geometry of the shell

In Figure 3 we show the image of the shell with circles centred on V1315 Aql overlaid. The radii of the circles are 100'', 180'' and 240''. The inner annulus between 100'' and 180'' contains the most prominent areas of emission (from the North around to the West), and appears to be centred on V1315 Aql. The outer annulus also contains a fainter arc of emission to the North-West, and some fainter areas of emission to the South-East, which also appear to be centred on V1315 Aql.

3.3 Keck DEIMOS spectra

In Figure 4 we show the spectrum of V1315 Aql. The spectrum shows strong, broad (FWHM of H α is 900 km s⁻¹) Balmer and HeI emission lines from the accretion disk. The spectrum is very similar to that shown in Dhillon & Rutten (1995).

3.3.1 Emission lines

The spectra of the seven shell slits and the blank sky slits in the range 6540–6600Å are shown in Fig. 5. Note that the blank sky 2 slit spanned two CCDs in the spectrograph and each part is shown separately. The shell spectra all show single-peaked emission lines of H α and a pair of N[II] lines at 6548 and 6583Å. These lines are characteristic of old nova shells (Downes et al. 2001).

We also detected H β in those shell spectra that covered 4861Å. Unfortunately, none of the spectra of the four flux-calibration stars covered this wavelength, and hence we were unable to flux calibrate the H β lines. We also found the S[II] 6716 and 6731Å lines in shell slits 2, 3, 5, 6 and 7, as shown in Figure 6. The average ratio of the two S[II] lines is 1:1.4.

We searched for the emission lines N[II] 5755Å, O[I] 6300, 6300, 6364Å and O[III] 4363, 4959, 5007Å, often seen in nova shell spectra, but none were detected. There are faint lines at 5679, 5740 and 5742Å, presumably from NI and NII, in shell slits 3 and 4, but these are not present in any other slits.

There is also H α emission present in both the sky portions of the slit centred on V1315 Aql, though any N[II]

lines present are lost in the noise. We show the H α line profile from the sky on the South-East side of the V1315 Aql slit in Figure 7.

The FWHM of the H α and N[II] lines of all the shell slits are listed in Table 3.

3.3.2 Systemic velocity of V1315 Aql

Historically the systemic velocity of V1315 Aql, γ , has been difficult to determine because of the complex behaviour of its disk emission lines and lack of absorption lines from the primary and secondary stars. Downes et al. (1986) presented radial velocity data for H β , H γ and HeII 4686Å emission lines. They derived values for γ consistent with zero from the H β and HeII 4686Å lines, but the H γ line gave a value of 100 km s⁻¹. Dhillon et al. (1991) also used the H β , H γ and HeII 4686Å emission lines and the HeI 4471Å line and derived a γ range of -4 to +93 km s⁻¹. Given the unreliability of the broad emission lines from the accretion disc to determine γ , in the following subsection we will use our own measurements of the radial velocity of the shell to determine if they are consistent.

3.3.3 Radial velocities of shell emission lines

To measure the radial velocities of the emission lines, we fitted a Gaussian to the H α line of the shell and measured the wavelength at the centre of the Gaussian. The resulting shell radial velocities are shown in Table 3.

The spectrum of the sky on the South-East side of the slit centred on V1315 Aql is shown in Figure 7. The plot shows tentative evidence of a double-peaked structure. We measured the radial velocity of each peak to be -33 and 14 km s⁻¹. If we assume that the two peaks represent emission from the front and back sides of a spherically-expanding shell, then the average of the two gives a systemic velocity of $\gamma \approx -10$ km s⁻¹, and an expansion velocity of ~ 25 km s⁻¹. We analysed the sky on the North-East side of V1315 Aql and it too showed a double-peaked structure, although it is less pronounced.

The seven shell slits were placed at the edges of the shell. The expansion velocity of the edge of the shell will be tangential to the line of sight and will not affect the radial velocities, which should be similar to the overall systemic velocity. The measured shell radial velocities are shown in Table 3 and are broadly comparable with the systemic velocity of -10 km s⁻¹ derived above, apart from shells 6 and 7 which differ by 14 and 16 km s⁻¹ respectively.

The Galactic velocity of V1315 Aql relative to the Sun can be derived from its Galactic coordinates, $l = 46.4^\circ$, $b = 0^\circ$, which give a radial velocity of 7 km s⁻¹. This is broadly consistent with the systemic velocity derived above.

3.3.4 Line fluxes

The fluxes of the emission lines from the shell in each of the slits are given in Table 4. Assuming a shell radius of 220'', a distance of 489 parsecs (Ak et al. 2008), and using the H α flux from each slit, we can estimate the total flux from the whole shell. However, we can see by examining Figure 3 that the shell is fragmented and clumpy and only a small fraction

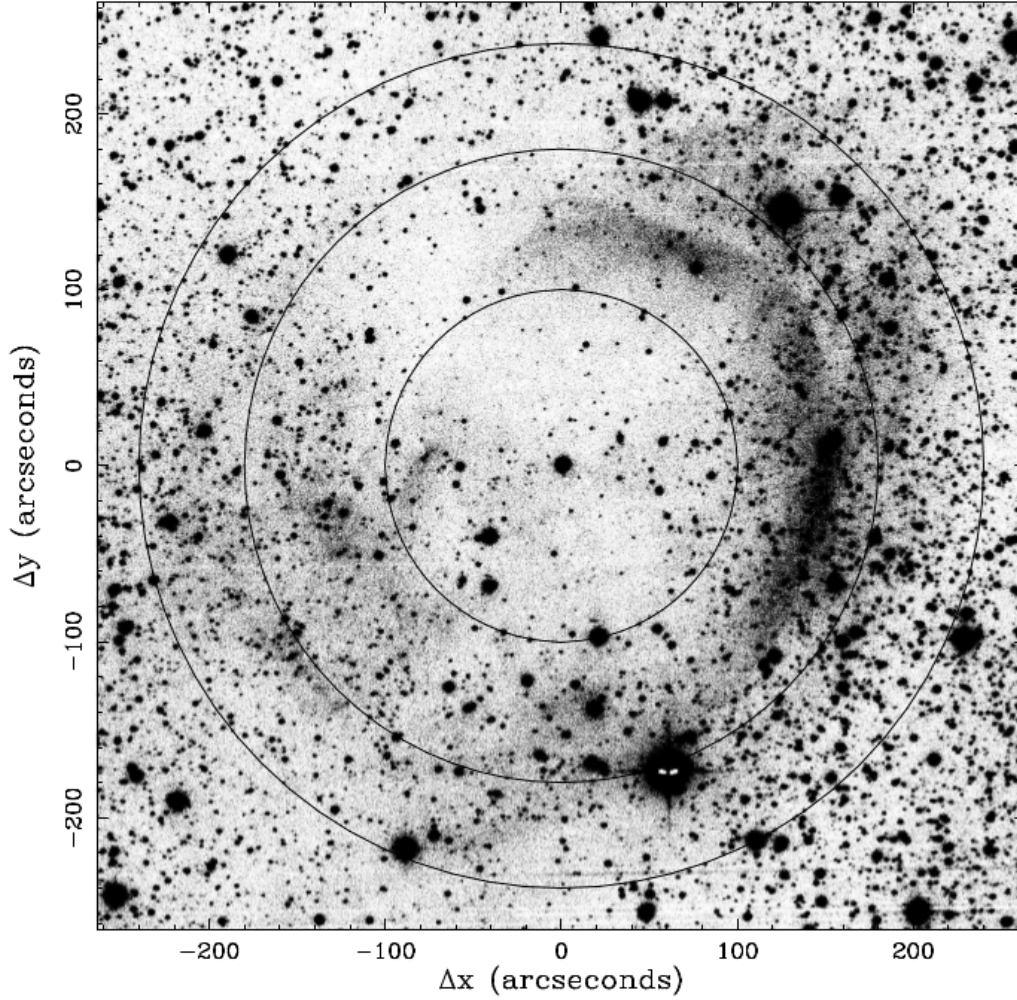


Figure 3. INT WFC $H\alpha$ image of the shell with overlaid circles centred on V1315 Aql of radii $100''$, $180''$ and $240''$. North is up and East is left.

Table 3. The first column shows the radial velocities in km s^{-1} of the $H\alpha$ emission line in the spectra of the seven V1315 Aql shell slits and the sky portion of the four flux calibration stars. The errors on the velocities are $\pm 5 \text{ km s}^{-1}$. The other columns shows the FWHM in km s^{-1} of each line. The errors on the FWHM are $\pm 8 \text{ km s}^{-1}$. The $H\alpha$ line in the V1315 Aql sky has a double peak and both radial velocities are shown. All values and errors were obtained from Gaussian fits to the emission lines.

Slit name	Radial Velocity	$H\alpha$	N[II] 6548Å	N[II] 6583Å	$H\beta$	NI 5676Å	NII 5740Å	NI 5742Å	SII 6716Å	SII 6731Å
Shell 1	-8	71	82	72	0	0	0	0	0	0
Shell 2	-8	86	65	74	0	0	0	0	67	78
Shell 3	-5	80	79	79	122	143	206	0	68	68
Shell 4	-3	79	59	75	89	78	0	124	0	0
Shell 5	-9	75	54	75	0	0	0	0	52	64
Shell 6	-26	84	87	80	0	0	0	0	78	76
Shell 7	4	89	87	86	0	0	0	0	91	84
V1315 Aql Sky	-33 & 14	0	0	0	0	0	0	0	0	0
Star 1	11									
Star 2	-23									
Star 3	29									
Star 4	14									

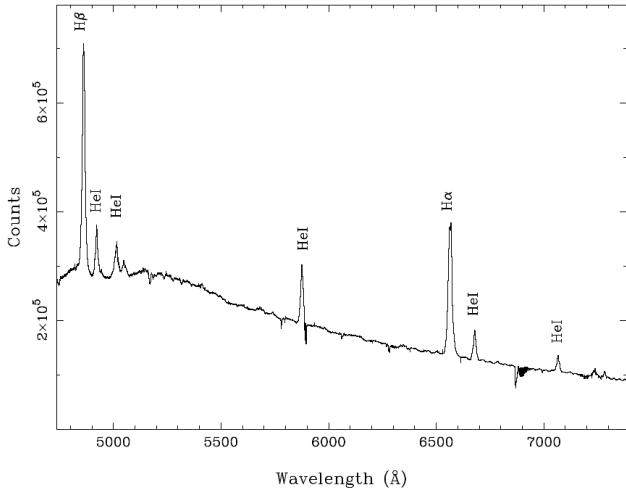


Figure 4. Keck DEIMOS spectrum of V1315 Aql. Note that we did not flux calibrate this spectrum because the flux calibration stars do not cover its whole wavelength range.

Table 4. $H\alpha$ and N[II] flux ($\text{ergs/s/cm}^2/\text{arcsec}^2 \times 10^{-18}$) from the seven shell slits. The errors on the flux values are $\pm 25\%$.

Shell slit No.	$H\alpha$	N[II] 6548Å	N[II] 6583Å
1	17.2	4.22	10.8
2	18.1	2.10	7.64
3	18.3	4.16	11.8
4	24.2	1.47	3.03
5	9.58	0.73	3.62
6	15.4	2.64	5.61
7	16.2	4.80	11.9

is actually emitting. If we assume that 10% of the full shell is emitting and take an average $H\alpha$ flux from the seven shell slits of $1.70 \times 10^{-17} \text{ ergs/cm}^2/\text{sec}/\text{arcsec}^2$, we obtain a total $H\alpha$ luminosity of $7.1 \times 10^{30} \text{ ergs/sec}$.

The plots of Downes et al. (2001) showing the temporal reduction in the $H\alpha$ luminosities of shells from fast and slow novae, have a lower limit of $\log L = 30$ at 100 yrs. We note that the source of the V1315 Aql luminosity is likely to include emission from shock interaction with pre-existing ISM. This would enhance the flux, and lead to an underestimate of the age of the shell. We conclude that the shell is likely to be significantly older than 100 yrs.

3.3.5 Time of nova eruption

The distance to V1315 Aql was measured by Ak et al. (2008) as $489 \pm 49 \text{ pc}$, computed from the Period-Luminosity-Colours (PLCs) relation of CVs calibrated with *2MASS* photometric data. The angular radius of the shell on our image is $\sim 4'$, giving a physical radius of $1.7 \times 10^{13} \text{ km}$. Duerbeck & Seitter (1987) found that the velocity of nova shells reduces by half every 50–100 yrs. Using our measured expansion velocity of $\sim 25 \text{ km s}^{-1}$, and assuming an initial velocity of $2,000 \text{ km s}^{-1}$ (see Table 8.1 Bode & Evans 2008), we estimate that the nova explosion occurred $\sim 500\text{--}600$ yrs ago.

However, if we take more extreme values for the initial ejection velocity, say 700 km s^{-1} and a deceleration half-life of 200 yrs then the age of the nova increases to 1,200 yrs.

Assuming the visual magnitude of V1315 Aql was the same prior to the nova event as it is now, $m_V = 14.3$, and taking the average brightening of a nova to be ~ 11 magnitudes (Bode & Evans 2008), the system would have been at $m_V \sim 3.3$ at peak brightness, clearly visible to the naked eye. Novae decline rapidly and so it would have dropped below the naked-eye visibility limit of $m_V \sim 6$ within a few days. We reviewed the catalogues of ancient Chinese and Asian novae and supernovae sightings by Stephenson (1976) which includes sightings from 532 BC up to 1604 AD. We could find no record of an event close to the coordinates of V1315 Aql. If the nova eruption occurred when V1315 Aql was close to the Sun in the sky, and it was brighter than $m_V \sim 6$ for only a few days, it may well have been hidden in twilight and hence gone unnoticed.

3.3.6 Temperature and density of the shell

The method most often used to determine the temperature and density of gaseous nebulae is to measure the ratio of the intensities of particular emission lines from the same species of ions. Two ions which are often used are N[II] and O[III]. We were unable to detect any O[III] lines in our spectra, and the N[II] ratio requires a flux measurement of the 5755Å line, which we were only able to detect very weakly in shell slit 1. It was not present in any other slit. Hence we can only place an upper limit on the electron temperature (T_e) of the shell of 5,000 K using Figure 5.1 from Osterbrock (1989).

3.3.7 Mass of the shell

We can derive a rough estimate of the mass of the shell using the technique set out in Corradi et al. (2015). They derived the ionised hydrogen masses of several planetary nebulae using the formula

$$m_{\text{shell}}(H^+) = \frac{4\pi D^2 F(H\beta) m_p}{h\nu_{H\beta} n_e \alpha_{H\beta}^{eff}(H^0, T_e)}, \quad (1)$$

where D is the distance to the object, $F(H\beta)$ is the $H\beta$ flux, m_p is the mass of a proton, $h\nu_{H\beta}$ is the energy of an $H\beta$ photon, n_e is the electron density per cm^3 , and $\alpha_{H\beta}^{eff}(H^0, T_e)$ is the effective recombination coefficient for $H\beta$. This formula is also applicable to nova shells (Osterbrock 1989).

As we pointed out in Section 3.3.1, the spectra of our four flux calibration stars do not cover $H\beta$ so we are unable to derive a flux directly. However, we can make a rough estimate as follows. The $H\beta$ line is present in four shell slits (Nos. 3, 4, 6 and 7). We can measure the counts for both $H\alpha$ and $H\beta$. The DEIMOS exposure time calculator for a source that is flat in frequency gives the ratio of counts for $H\alpha:H\beta$ as approximately 1:0.3. Assuming that 10% of the full shell is emitting and taking an average $H\alpha$ flux from the seven shell slits of $1.70 \times 10^{-17} \text{ ergs/cm}^2/\text{sec}/\text{arcsec}^2$ we obtain a total $H\alpha$ flux of $2.49 \times 10^{-13} \text{ ergs/cm}^2/\text{sec}$ from the whole shell, allowing us to derive an $H\beta$ flux of $F(H\beta) = 8.9 \times 10^{-14} \text{ ergs/cm}^2/\text{sec}$.

The electron density, n_e , can be estimated using the S[II] 6716 and 6731 line ratio, which we found to be 1.4 (see

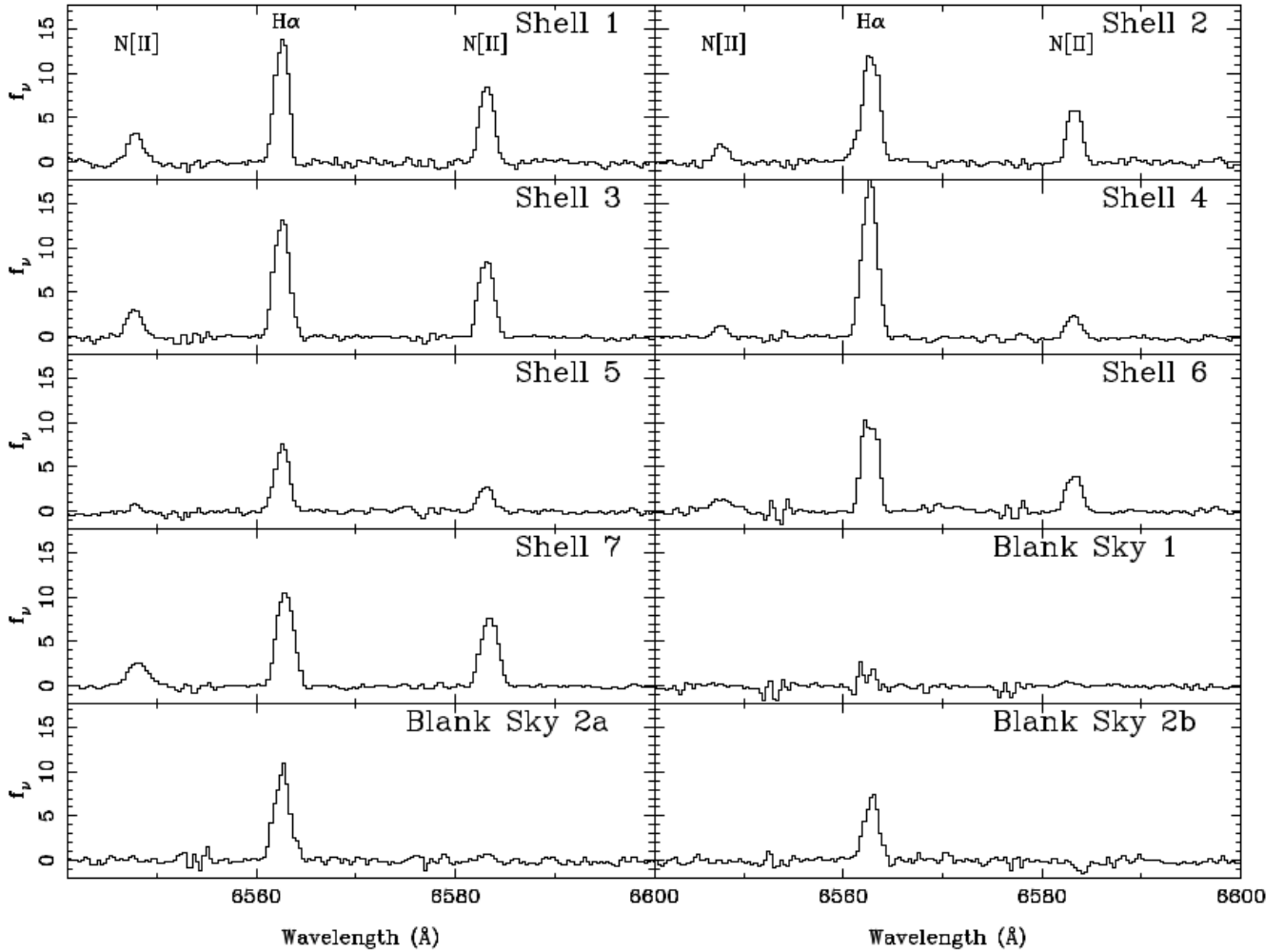


Figure 5. Spectra of the seven shell slits (see Fig. 2), and the blank sky slits from 6540–6600Å. The flux is in units of $\mu\text{Jy arcsec}^{-2}$. The slit spectra all show the presence of H α and N[II] 6548Å and N[II] 6583Å. H α is also present in the blank sky slits. The Blank Sky 2 slit fell across two CCDs on the detector and so we show each spectrum separately, as 2a and 2b.

Section 3.3.1). Figure 5.8 in Osterbrock (1989) shows the electron density versus intensity ratio at $T_e = 10,000$ K and indicates a scaling of $n_e(10^4/T_e)^{1/2}$. We found a maximum temperature of 5,000 K which gives an electron density of $\sim 22 \text{ cm}^{-3}$.

Finally, using the distance measured by Ak et al. (2008) of 489 pc and a value for $\alpha_{\text{H}\beta}^{\text{eff}}(H^0, T_e)$ of 3.78×10^{-14} , for Case A conditions at $T_e = 5000$ K listed in Table 4.1 of Osterbrock (1989) gives a maximum mass of

$$m_{\text{shell}}(H^+) \simeq 2 \times 10^{-4} M_{\odot}. \quad (2)$$

There is no need to correct for extinction as Rutten et al. (1992) found $E(B - V) = 0$ for V1315 Aql using *IUE* spectra of interstellar absorption bands around 2200Å. In view of the many assumptions used to estimate the mass of the shell, it should be treated as an order of magnitude approximation.

As nova shells expand they decelerate as they sweep up pre-existing circumstellar gas, which leads to a doubling of their mass every 50–100 yrs (Duerbeck & Seitter 1987). We estimated the age of the shell in Section 3.3.5 as 500–1200 yrs, so the original ejected mass of the shell would have been

substantially lower than the value we have derived above, giving a maximum ejected mass of $\lesssim 10^{-5} M_{\odot}$. This rules out a planetary nebula origin, which typically have masses in the range 0.1–1.0 M_{\odot} (Osterbrock 1989). Nova shells typically have masses in the range 10^{-4} – $10^{-6} M_{\odot}$ (Yaron et al. 2005), so our estimate of the shell mass in V1315 Aql of $\sim 10^{-5} M_{\odot}$ is in accordance with this.

4 DISCUSSION

We can summarise our findings as follows. The shell is broadly spherical and appears to be centred on V1315 Aql, strongly suggesting that the shell is associated with the central binary. The systemic velocity of the shell measured from the sky portion of the V1315 Aql slit and at the edges of the shell are broadly consistent. The absence of 22 μm emission precludes a planetary nebula origin (Mizuno et al. 2010). We derive an order-of-magnitude estimate of the mass of the shell of $\sim 10^{-5} M_{\odot}$ which rules out a planetary nebula or supernova origin. We conclude that these results indicate that the shell is associated with V1315 Aql.

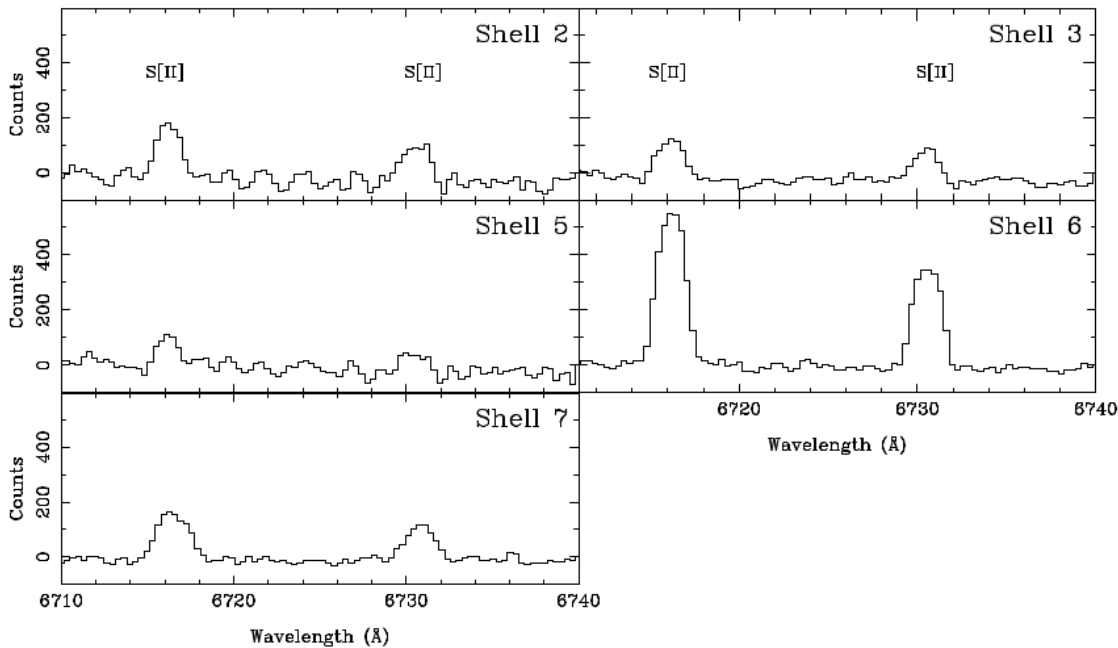


Figure 6. Spectra of the five shell slits from 6710–6740Å showing the S[II] emission lines at 6716 and 6731Å.

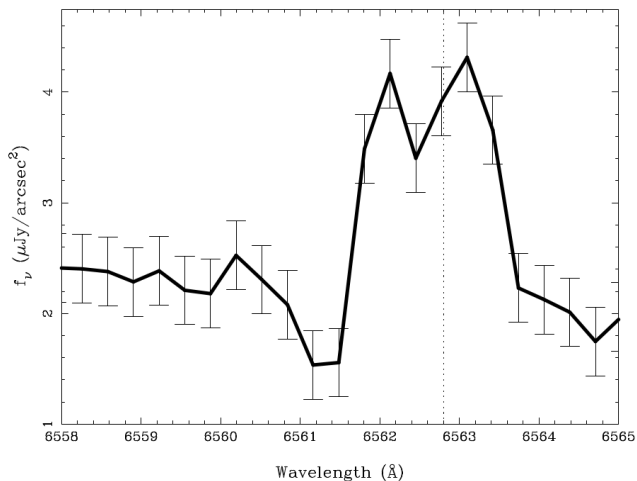


Figure 7. H α spectrum of the sky from the South-East side of the V1315 Aql slit. The error bars show the noise levels of the background sky

At this stage of the shell’s evolution, the luminosity of the outer edges of the shell is most likely fuelled by two processes, recombination and shock interaction with pre-existing CSM. Our flux measurement will include contributions from both of these processes, making it difficult to estimate the physical conditions in the shell as a whole. Furthermore, the lack of other forbidden emission lines in the shell spectra, especially N[II] 6583Å and O[II], means we cannot determine the physical parameters of the shell to confirm conclusively that it exhibits properties consistent with a nova origin.

In S15, we estimated that the nova-like phase following a nova eruption lasts ~ 2400 yrs. This is comparable to

the ~ 2000 yrs order-of-magnitude estimate by Patterson et al. (2013), based on the transition of BK Lyn to a dwarf nova in the year 2011. However, the AAVSO light curve of BK Lyn⁴ suggests that it has now reverted back to a nova-like state, indicating that the object is a Z Cam-type dwarf nova that has likely been transitioning from the nova-like to dwarf nova state for much less than the ~ 2000 -yr estimate of Patterson et al. (2013). Shara et al. (2017) found that the transition time for AT Cnc was much shorter at 330^{+135}_{-90} yrs. Our estimate of the time since the nova eruption on V1315 Aql of 500–1200 yrs is consistent with both these timescales, and lies within the overall nova recurrence timescale of 13000 yrs found by Schmidtbreick et al. (2015).

5 CONCLUSIONS

We present images and spectra of the shell surrounding V1315 Aql. Our results strongly suggest that the shell originated from a nova eruption on the CV. This discovery of the first nova shell around a nova-like variable adds further support to the theory of nova-induced cycles in the mass transfer rates of CVs.

ACKNOWLEDGMENTS

We would like to thank the referee for his helpful comments and for pointing out the latest AAVSO light curve of BK Lyn demonstrating Z Cam-like behaviour.

VSD and SPL were supported under grants from the Science and Technology Facilities Council (STFC). This

⁴ <https://www.aavso.org/>

publication makes use of VOSA, developed under the Spanish Virtual Observatory project supported from the Spanish MICINN through grant AyA2011-24052. The INT is operated on the island of La Palma by the Isaac Newton Group of Telescopes in the Spanish Observatorio del Roque de los Muchachos of the Instituto de Astrofísica de Canarias. Some of the data presented herein were obtained at the W.M. Keck Observatory, which is operated as a scientific partnership among the California Institute of Technology, the University of California and the National Aeronautics and Space Administration. The Observatory was made possible by the generous financial support of the W.M. Keck Foundation. The authors wish to recognise and acknowledge the very significant cultural role and reverence that the summit of Mauna Kea has always had within the indigenous Hawaiian community. We are most fortunate to have the opportunity to conduct observations from this mountain.

REFERENCES

- Ak T., Bilir S., Ak S., Eker Z., 2008, *New Astronomy*, 13, 133
- Bayo A., Rodrigo C., Barrado Y Navascués D., Solano E., Gutiérrez R., Morales-Calderón M., Allard F., 2008, *A&A*, 492, 277
- Bianchi L., 2014, *Ap&SS*, 354, 103
- Bode M. F., Evans A., 2008, *Classical Novae*. Cambridge University Press
- Büning A., Ritter H., 2004, *A&A*, 423, 281
- Corradi R. L. M., García-Rojas J., Jones D., Rodríguez-Gil P., 2015, *ApJ*, 803, 99
- Dhillon V. S., Marsh T. R., Jones D. H. P., 1991, *MNRAS*, 252, 342
- Dhillon V. S., Rutten R. G. M., 1995, *MNRAS*, 277, 777
- Downes A. R., Matteo M., Szkody P., Jenner D. C., Margon B., 1986, *ApJ*, 301, 240
- Downes R. A., Duerbeck H. W., Delahodde C. E., 2001, *Journal of Astronomical Data*, 7, 6
- Duerbeck H. W., Seitter W. C., 1987, *Astrophys. Sp. Sci.*, 131, 467
- Faber S. M., Phillips A. C., Kibrick R. I., Alcott B., Allen S. L., Burrous J., Cantrall T., Clarke D., Coil A. L., Cowley D. J., Davis M., Deich W. T. S., Dietsch K., Gilmore D. K., Harper C. A., Hilyard D. F. e. a., 2003, in Iye M., Moorwood A. F. M., eds, *Instrument Design and Performance for Optical/Infrared Ground-based Telescopes* p. 1657
- Hardy L. K., Butterley T., Dhillon V. S., Littlefair S. P., Wilson R. W., 2015, *MNRAS*, 454, 4316
- Knigge C., 2010, *AIP Conference Proceedings*, 1314, 171
- Knigge C., Baraffe I., Patterson J., 2011, *ApJS*, 194, 28
- Mizuno D. R., Kraemer K. E., Flagey N., Billot N., Shenoy S., Paladini R., Ryan E., Noriega-Crespo A., Carey S. J., 2010, *AJ*, 139, 1542
- Osaki Y., 1974, *Pub. Astr. Soc. Japan*, 26, 429
- Osterbrock D. E., 1989, *Astrophysics of gaseous nebulae and active galactic nuclei*. University Science Books, Sausalito, California
- Patterson J., Uthas H., Kemp J., de Miguel E., Krajci T., Foote J., Hamsch F.-J., Campbell T., Roberts G., Cejudo D., Dvorak S., Vanmunster T., Koff R., Skillman D., Harvey D., Martin B., Rock J., Boyd D., Oksanen A., Morelle E., Ulowetz J., Kroes A., Sabo R., Jensen L., 2013, *MNRAS*, 434, 1902
- Rodríguez-Gil P., Gänsicke B. T., Hagen H.-J., Araujo-Betancor S., Aungwerojwit A., Allende Prieto C., Boyd D., Casares J., Engels D., Giannakis O., Harlaftis E. T., Kube J., Lehto H. e. a., 2007, *MNRAS*, 377, 1747
- Rutten R. G. M., van Paradijs J., Tinbergen J., 1992, *A&A*, 260, 213
- Sahman D. I., Dhillon V. S., Knigge C., Marsh T. R., 2015, *MNRAS*, 451, 2863
- Schmidtobreick L., Shara M., Tappert C., Bayo A., Ederoclite A., 2015, *ArXiv e-prints*, p. 1502.05230
- Shara M. M., Drissen L., Martin T., Alarie A., Stephenson F. R., 2017, *MNRAS*, 465, 739
- Shara M. M., Ilkiewicz K., Mikolajewska J., Pagnotta A., Bode M. F., Crause L. A., Drozd K., Faherty J. K., Fuentes-Morales I., Grindlay J. E., Moffat A. F. J., Schmidtobreick L., Stephenson F. R., Tappert C., Zurek D., 2017, *ArXiv e-prints*, p. 1704.00086
- Shara M. M., Livio M., Moffat A. F. J., Orio M., 1986, *ApJ*, 311, 163
- Shara M. M., Martin C. D., Seibert M., Rich R. M., Salim S., Reitzel D., Schiminovich D., Deliyannis C. P., Sarrazine A. R., Kulkarni S. R., Ofek E. O., Brosch N., Lépine S., Zurek D., De Marco O., Jacoby G., 2007, *Nat*, 446, 159
- Shara M. M., Mizusawa T., Wehinger P., Zurek D., Martin C. D., Neill J. D., Forster K., Seibert M., 2012, *ApJ*, 758, 121
- Skrutskie M. F., Cutri R. M., Stiening R., Weinberg M. D., Schneider S., Carpenter J. M., Beichman C., Capps R., Chester T., Elias J., Huchra J., Liebert J., Lonsdale C., Monet D. G., Price S., Seitzer P., Jarrett T., Others ., 2006, *ApJ*, 131, 1163
- Stephenson F. R., 1976, *QJRAS*, 17, 121
- Warner B., 1995, *Cataclysmic Variable Stars*. Cambridge University Press, Cambridge
- Wright E. L., Eisenhardt P. R. M., Mainzer A. K., Ressler M. E., Cutri R. M., Jarrett T., Kirkpatrick J. D., Padgett D., McMillan R. S., Skrutskie M., Stanford S. A., Cohen M., Walker R. G., Mather J. C., Leisawitz D. e. a., 2010, *AJ*, 140, 1868
- Yaron O., Prialnik D., Shara M. M., Kovetz A., 2005, *ApJ*, 623, 398